Biofabrication

International Society for Biofabrication

PAPER

Bioprinting of dual ECM scaffolds encapsulating limbal stem/progenitor cells in active and quiescent statuses

To cite this article: Zheng Zhong *et al* 2021 *Biofabrication* **13** 044101

IOP Publishing Biofabrication 13 (2021) 044101 https://doi.org/10.1088/1758-5090/ac1992

Biofabrication

PAPER

Bioprinting of dual ECM scaffolds encapsulating limbal stem/progenitor cells in active and quiescent statuses

Zheng Zhong[1], Alis Balayan[1,2], Jing Tian[3], Yi Xiang[1], Henry H Hwang[1], Xiaokang Wu[2], Xiaoqian Deng[2], Jacob Schimelman[1], Yazhi Sun[1], Chao Ma[4], Aurelie Dos Santos[4], Shangting You[1], Min Tang[1], Emmie Yao[1], Xiaoao Shi[3], Nicole F Steinmetz[1], Sophie X Deng[4,*] and Shaochen Chen[1,3,*]

[1] Department of NanoEngineering, University of California San Diego, La Jolla, CA 92093, United States of America
[2] School of Medicine, University of California San Diego, La Jolla, CA 92093, United States of America
[3] Department of Bioengineering, University of California San Diego, La Jolla, CA 92093, United States of America
[4] Stein Eye Institute, University of California Los Angeles, Los Angeles, CA 90095, United States of America
[*] Authors to whom any correspondence should be addressed.

E-mail: chen168@eng.ucsd.edu **and** deng@jsei.ucla.edu

RECEIVED
20 January 2021

REVISED
16 July 2021

ACCEPTED FOR PUBLICATION
30 July 2021

PUBLISHED
13 August 2021

Keywords: DLP-based bioprinting, limbal stem cell, stem cell quiescence, endogenous stem cell, hyaluronic acid, regenerative medicine

Supplementary material for this article is available online

Abstract

Limbal stem cell deficiency and corneal disorders are among the top global threats for human vision. Emerging therapies that integrate stem cell transplantation with engineered hydrogel scaffolds for biological and mechanical support are becoming a rising trend in the field. However, methods for high-throughput fabrication of hydrogel scaffolds, as well as knowledge of the interaction between limbal stem/progenitor cells (LSCs) and the surrounding extracellular matrix (ECM) are still much needed. Here, we employed digital light processing (DLP)-based bioprinting to fabricate hydrogel scaffolds encapsulating primary LSCs and studied the ECM-dependent LSC phenotypes. The DLP-based bioprinting with gelatin methacrylate (GelMA) or hyaluronic acid glycidyl methacrylate (HAGM) generated microscale hydrogel scaffolds that could support the viability of the encapsulated primary rabbit LSCs (rbLSCs) in culture. Immunocytochemistry and transcriptional analysis showed that the encapsulated rbLSCs remained active in GelMA-based scaffolds while exhibited quiescence in the HAGM-based scaffolds. The primary human LSCs encapsulated within bioprinted scaffolds showed consistent ECM-dependent active/quiescent statuses. Based on these results, we have developed a novel bioprinted dual ECM 'Yin-Yang' model encapsulating LSCs to support both active and quiescent statues. Our findings provide valuable insights towards stem cell therapies and regenerative medicine for corneal reconstruction.

1. Introduction

Corneal epithelium is a transparent nonkeratinized epithelium that contributes to the refractive power of eye and serves as the first protective barrier against the outside world [1, 2]. Limbal stem/progenitor cells (LSCs) are endogenous stem cells that reside at the limbus, the periphery of the cornea [3]. LSCs are responsible for the homeostasis of corneal epithelium, thus, facilitating optical clarity and light transmission [2, 3]. Worldwide, there are over 5 million individuals affected by corneal blindness and limbal stem cell deficiency (LSCD) being a common etiology [4–6]. Conventional LSCD treatments employ surgical repair interventions using such sources as amniotic membrane (AM) as substrate or scaffold combined with keratolimbal autografts, or allografts [7]. These treatment approaches are limited by the lack of standardized preparation of AM, risk of developing iatrogenic LSCD and immunologic rejection [8–10].

Recent advances in regenerative medicine and tissue engineering have facilitated the development of novel transplantation approaches using advanced biomaterials for the treatment of LSCD [11]. Hydrogel scaffolds based on collagen, gelatin, hyaluronic acid (HA), and synthetic polymers have

been investigated as LSC carriers for transplantation [12–15]. Among the various approaches of hydrogel scaffold fabrication, digital light processing (DLP)-based bioprinting stands out as a high-throughput platform allowing fabrication of hydrogel scaffolds that support the encapsulation of numerous types of stem cells including retinal progenitor cells, conjunctival stem cells, mesenchymal stem cells, neural progenitor cells and cancer stem cells [16–21]. The spatiotemporal control of light exposure afforded by DLP-based bioprinting also enables the stiffness tunability within desired regions of the fabricated hydrogel scaffolds, thus allowing one to manipulate the phenotypes of the encapsulated cells [19, 22–25]. Moreover, DLP-based bioprinting enables the use of multiple extracellular matrix (ECM) components and multiple cell types during hydrogel fabrication to better recapitulate the complex native microenvironment of stem cells [16, 17, 26].

Biological and biomechanical interactions between stem cells and their ECM have been shown to affect cell fate and phenotype [27–29]. Biomechanical factors such as substrate stiffness have been shown to regulate the activities of LSCs and the corneal regeneration under physiological and pathological conditions [30]. Stem cells can also interact with the scaffolds in a composition-dependent way as various types of cell surface receptors responding to the ECM by triggering downstream intracellular signaling pathways that dynamically and comprehensively manipulate cell programming [12, 31–35]. The delicate balance between activation and quiescence of endogenous stem cells, including LSCs, is critical for the system homeostasis under varying healthy, aging, and diseased circumstances [34, 36, 37]. Recent studies have showed that engineered scaffolds are able to tune the transition of activation/quiescence in LSCs [33, 38]. Therefore, understanding how the different ECM compositions regulate LSCs in a 3D microenvironment is important for developing novel transplantable LSC scaffolds.

In this study, we present a bioprinting approach in fabricating primary LSC-encapsulated microscale hydrogel scaffolds to study the ECM-dependent LSC activities. With the customized DLP-based bioprinting system, we fabricated microscale hydrogel scaffolds with gelatin methacrylate (GelMA) and hyaluronic acid glycidyl methacrylate (HAGM) that supported the encapsulation and cell viability of primary rabbit LSCs (rbLSCs). Next, we analyzed the different phenotypes of encapsulated rbLSCs at mRNA and protein levels. In addition, we extended the study on primary human LSCs (hLSCs) from different individuals with bioprinting. Furthermore, we performed multimaterial bioprinting and fabricated a dual ECM 'Yin-Yang' model encapsulating primary rbLSCs in active/quiescent status. Overall, we developed an innovative DLP-based bioprinting approach for LSC engineering while broadening the understanding of ECM-dependent LSCs phenotypes, which is a meaningful step towards the development of regenerative medicine for LSCD and other severe ocular surface diseases.

2. Materials and methods

2.1. Primary rabbit, hLSCs isolation and culture

The rabbit tissues from 10 to 12 weeks old New Zealand White rabbit eyes (*Oryctolagus Cuniculus*) were acquired from Sierra for Medical Science, Inc. (Whittier, CA). The human corneoscleral rims were acquired from One Legacy or Saving Sight eye banks. Consent was obtained by the eye banks for the tissues to be used for research. Experimentation on human tissue adhered to the tenets of the Declaration of Helsinki. The protocol for human corneal tissue collection and dissection was evaluated and exempted by the University of California, Los Angeles (UCLA) Institutional Review Boards (IRB#12-000363). The overall procedure was approved by University of California San Diego Institutional Biosafety Committee.

For rbLSCs, rabbit eyeballs were washed in Dulbecco's phosphate-buffered saline (DPBS) and Dulbecco's modified eagle medium (DMEM, ThermoFisher Scientific) with penicillin-streptomycin, respectively, and the corneoscleral rims were isolated for further dissection. hLSCs were harvested from donor corneoscleral rims stored in Optisol-GS. Corneoscleral rims from three different donors with no significant history of corneal diseases were used in this study. The isolation of both rbLSCs and hLSCs was performed as previously described [2]. Briefly, limbal epithelium with underlying stroma was excised circumferentially and minced using Vannas scissors. Type IV collagenase (0.2%, Sigma Aldrich) was used for digestion at 37 °C with constant shaking at 120 rpm for 1–1.5 h. Following the incubation, cells were pelleted and washed with PBS. Following a 10 min digestion using 0.25% Trypsin-EDTA (ethylenediamine tetraacetic acid) (Sigma Aldrich), the cells were filtered through a 70 μm cell strainer (Corning) to obtain single cells. The cells were seeded onto Collagen I coated plates (ThermoFisher Scientific). The culture medium used was composed of DMEM /F-12 (3:1, ThermoFisher Scientific) with 10% fetal bovine serum (ThermoFisher Scientific), penicillin-streptomycin (ThermoFisher Scientific), 400 ng ml^{-1} hydrocortisone (Sigma Aldrich), 1× insulin-transferrin-selenium (Corning), 2 nM reverse T3 (Sigma Aldrich), and 0.1 nM cholera toxin (Sigma Aldrich), 10 ng ml^{-1} epidermal growth factor (EGF, R&D System), and 10 μM Y27632 (Tocris Bioscience).

2.2. Material synthesis and photocrosslinkable bioink preparation

The synthesis process of GelMA and HAGM was performed following previously established protocols

[16, 17, 19, 26, 39]. Briefly, for GelMA, a 10% (w/v) gelatin solution was prepared by dissolving porcine skin gelatin type A (Sigma Aldrich) in a 0.25 M carbonate-bicarbonate (3:7) buffer at pH 9 while stirring at 50 °C. Methacrylic anhydride (Sigma Aldrich) was then mixed in a dropwise fashion to the gelatin solution to reach 100 μl methacrylic anhydride per gram of gelatin. Then, following 1 h of continuous stirring at 50 °C, the product was subjected to overnight fluid dynamic dialysis using 13.5 kDa dialysis tubes (Repligen). Lyophilization for three days was then conducted to produce GelMA powder which was then stored at −80 °C. The degree of methacrylation of the resultant GelMA is approximately 95% [17].

To synthesize HAGM, 1.0 g of sodium hyaluronate (Lifecore Biomedical) was dissolved in 100 ml water: acetone solution (1:1 ratio) and stirred at room temperature overnight to prepare a 1% (w/v) HA solution. The flask was subjected to vacuum for 3 s or until the solution boils then flooded with Argon. This step was repeated twice and the solution was stirred overnight protected from light. On the next day, 7.2 ml triethylamine (Sigma Aldrich) 20-fold in excess was slowly added to the reaction flask until thoroughly mixed. The reaction was then flooded with argon gas, then immediately sealed, and mixed for 30 min. Using a syringe, 7.2 ml of glycidyl methacrylate (GM, Sigma Aldrich) in 20-fold excess was added dropwise to the reaction. Afterwards, the reaction was flooded with Argon, sealed, and stirred overnight at room temperature. The resulting material was precipitated using acetone and vacuum filtration was used to collect the precipitate which was dissolved in DI water. The dissolved material was then dialyzed, lyophilized, and stored at −80 °C until further use. The degree of methacrylation of the resultant HAGM is approximately 35% [17].

For photopolymerization, lithium phenyl-2,4,6-trimethylbenzoylphosphinate (LAP) was used as a photoinitiator and synthesized per previously published protocols [16, 19]. Briefly, dimethyl phenylphosphonite (18 mmol, Sigma Aldrich) was added dropwise to an equimolar 2,4,6-trimethylbenzoyl chloride (Acros Organics). The reaction was constantly stirred for 18 h at room temperature. A solution of lithium bromide (6.1 g, Sigma Aldrich) in 100 ml of 2-butanone (Sigma Aldrich) was then mixed into the reaction. Following a 10 min stirring at 50 °C, the mixture was incubated overnight at room temperature. Filter-washing with 2-butanone for three times was carried out to remove unreacted lithium bromide. The LAP solids that resulted from the reaction were crushed into powder and stored under argon in the dark at 4 °C.

About 8% (w/v) GelMA with 0.25% (w/v) LAP and 4% (w/v) HAGM with 0.25% (w/v) LAP were dissolved in warm DPBS, filtered using a 0.22 μm syringe and used as prepolymer solutions for DLP-based bioprinting with or without LSCs. The cells were detached from the culture plates with 0.25% trypsin-EDTA, and then neutralized with a pre-made culture medium. The cell solution was then filtered with a 70 μm cell strainer and the cell concentration was measured with a hemocytometer. The bioink containing 1–2 $\times$ 10^7 cells ml^{-1} LSCs and GelMA/HAGM prepolymer solution was prepared right before printing.

2.3. Bioprinting of GelMA and HAGM hydrogel scaffolds

Our in-house DLP-based bioprinting system was used for the rapid biofabrication of hydrogel scaffolds. The system is composed of a 365 nm light source (Hamamatsu), a projection optics assembly, a motion-controlled stage (Newport) and a digital micromirror device (DMD, Texas Instruments.) used for patterning the light. We generated digital patterns using Adobe photoshop which were imported into the custom operation software that controls the DMD chip to modulate light projection depending on the imported pattern. For the bioprinting setup, two polydimethylsiloxane (PDMS) spacers with thickness of 250 μm were set between a PDMS base that is attached to a glass slide and a methacrylated coverslip. This creates a gap of desired thickness where the prepolymer bioink was loaded. Then, photopolymerization was performed with the DLP bioprinter and the printed constructs were immediately moved to a 24-well plate and washed in pre-warmed DPBS to remove the excess bioink materials. The DPBS was then substituted with warmed culture medium and the bioprinted constructs were incubated in 5% CO_2 at 37 °C.

2.4. Immunofluorescence staining

Primary LSCs cultured on Millicell EZ slides (Millipore Sigma) were washed twice with DPBS to prepare for 2D cell staining. The cells were fixed at room temperature for 20 min with 4% (w/v) paraformaldehyde (FUJIFILM Wako), followed by three washes with DPBS, each for 10 min. Then, the samples underwent blocking and permeabilization for 1 h using 5% bovine serum albumin (Sigma Aldrich) and 0.3% triton X-100 (Sigma Aldrich) in DPBS at room temperature. Primary antibody incubation was done at 4 °C overnight followed by three DPBS washes for 10 min each. Afterwards, the cells were incubated with secondary antibodies (Alexa Fluor-conjugated, Invitrogen) for 1 h at room temperature. The samples were further washed with DPBS and nuclear staining was done with 1:500 4′,6-diamidino-2-phenylindole (ThermoFisher Scientific) in DPBS for 10 min. After a final DPBS wash the samples were left to air-dry for 30 s and mounted with Fluoromount-G™ Mounting Medium (ThermoFisher Scientific). Hydrogel cells

staining was performed with the exact same procedure, except without mounting, where the samples were left in DPBS to be imaged. The samples were all imaged within 48 h of staining to preserve clarity. Further information on details of antibodies and dilution rates is provided in supplementary table 1 (available online at stacks.iop.org/BF/00/00000/mmedia).

2.5. Mechanical properties characterization

A micromechanical testing machine (Microsquisher, CellScale) was used to determine the Young's modulus of the bioprinted scaffolds based on GelMA and HAGM. Cylindrical test specimens (500 μm diameter, 500 μm height) printed with 8% GelMA or 4% HAGM were fabricated and incubated at 37 °C for overnight. We followed the manufacturer's instructions when measuring the compressive modulus. The sample's hysteresis was removed using two cycles of predetermined compression. During mechanical testing, the samples were compressed at a 10% strain with a strain rate of 2 μm s^{-1}. After the force and displacement data was collected from the Microsquisher, we used custom MATLAB script to calculate the compressive Young's modulus.

2.6. Viability evaluation

The viability of the LSCs encapsulated in the hydrogels were studied with the viability/cytotoxicity kit (Thermo Fisher), also known as Live/Dead™ staining. They were incubated with 2 μM calcein acetoxymethyl ester, along with 4 μM ethidium homodimer in DPBS, for 30 min at 37 °C. Fluorescent imaging was done with a Leica microscope (DMI 6000-B). The viability test was carried out in triplicates.

2.7. RNA isolation, reverse transcription, and real time quantitative PCR

For RNA extraction, a TRIzol® reagent (Ambion Thermo Fisher) was continuously pipetted into the pelleted 2D-cultured cells. For the encapsulated LSCs in GelMA- and HAGM-based bioprinted hydrogel scaffolds, the constructs were stripped off their coverslips using a scalpel and subjected to enzymatic digestion with 0.2% Type IV collagenase (Sigma Aldrich) and 1kU/ml hyaluronidase (STEMCELL Technologies), respectively, at 37 °C for 15 min. The resulting cell solution was pelleted with centrifugation immediately followed by addition of TRIzol® reagent to the pellet. The lysate was then used directly or stored in −80 °C. Direct-zol™ RNA Purification kit (Zymo Research) was used for the extraction of RNA following the manufacturer's protocol. NanoDrop™ 2000 (Thermo Fisher Scientific) was used to quantify the purified RNA. The RNA was then used for cDNA synthesis and reverse transcription using the iScript™ cDNA Synthesis Kit (Bio-Rad) with thermal cycler StepOne™ Real-Time PCR System (Thermo Fisher Scientific). Luna® Universal qPCR Master Mix was used for real-time quantitative polymerase chain reaction (qPCR). The primer details used in the qPCR can be found in supplementary table 2.

2.8. Flow cytometry

For flow cytometry, GelMA- and HAGM-based bioprinted scaffolds were enzymatically digested to isolate the encapsulated LSCs. Following the enzymatic digestion, the cells extracted from the scaffolds and 2D-cultured cells were digested with 0.25% trypsin-EDTA and filtered with a 70 μm cell strainer. After centrifugation, cell pellets were resuspended and fixed with Cytofix™ Fixation Buffer (BD) for 20 min followed by three 5 min wash with Cell Staining Buffer (Biolegend) supplemented with 0.2% triton X-100. Primary antibodies were diluted with Cell staining buffer and applied for 20 min. Following a wash, secondary antibodies were diluted with cell staining buffer and applied for 20 min. All the antibody incubations were performed at room temperature. Cell solutions were then kept on ice in the dark until use. The propidium iodide (Biolegend) viability staining was performed following the manufacturer's procedures. Briefly, 10 μl per million cells of the propidium iodide solution was added to the cell suspension. The solution was then incubated for 15 mins at 4 °C avoiding light before analysis. Flow cytometry was performed using BD Accuri™ C6 flow cytometer following the instructions of the manufacturer. The data was collected from at least 100 000 events for each group and processed using FlowJo.

2.9. Imaging and processing

Confocal and brightfield/regular fluorescence imaging of the samples were taken using SP8 Confocal and DMI 6000-B Leica microscopes, respectively. ImageJ and LAS X were used to further process the images.

2.10. Statistical analysis

Data obtained from the experiments were processed with Microsoft Excel and presented in a way of mean ± standard deviations Student's t-test (two tailed) or one-way ANOVA were applied to determine statistical significance which was denoted on the figures with an asterisk where appropriate ($^{*}P < 0.05$; $^{**}P < 0.01$; $^{***}P < 0.001$.).

3. Results

3.1. Bioprinted GelMA and HAGM hydrogel scaffolds supported the viability of encapsulated primary rbLSCs

Our customized DLP-based bioprinting system can spatially manipulate light based on

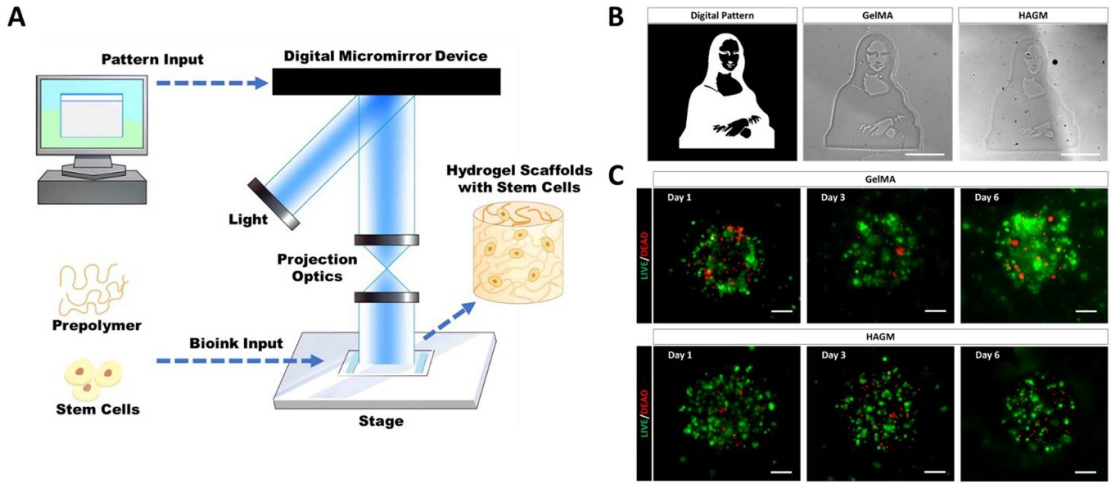

Figure 1. Bioprinting of GelMA- or HAGM-based scaffolds encapsulating primary rbLSCs. (A) Schematic of DLP-based bioprinting workflow; (B) representative bright field images of bioprinted Mona Lisa with acellular GelMA or HAGM; (C) representative images of Live/Dead^{TM} staining of rbLSCs encapsulated with GelMA- or HAGM-based bioprinted scaffolds at day 1, day 3 and day 6 of culture (scale bars: 100 μm).

user-defined input designs, allowing for precise photopolymerization-based patterning of cellularized hydrogel constructs containing different material compositions (figure 1(A)) [18, 19, 24]. GelMA is a photocrosslinkable gelatin that has been extensively studied as a bioink for the bioprinting of stem cells including conjunctival stem cells and mesenchymal stem cells [19, 40]. HAGM as another photocrosslinkable bioink, was found to support the encapsulation of retinal progenitor cells and cancer stem cells [16, 17]. Using DLP-based bioprinting techniques, we were able to fabricate GelMA- or HAGM-based hydrogel scaffolds with a complex pattern and microscale resolution within a matter of seconds (figure 1(B)). To encapsulate LSCs in 3D scaffolds, we isolated and expanded the primary rbLSCs from fresh rabbit limbal tissues and characterized with immunofluorescence staining of various LSC markers (supplementary figure S1(A)). To test biocompatibility, we fabricated GelMA- or HAGM-based bioprinted scaffolds encapsulating primary rbLSCs. The Live/Dead^{TM} staining confirmed that both types of bioprinted scaffolds were able to support the viability of the encapsulated rbLSCs after seven days of culture (figure 1(C)). We have also quantified the viability of the encapsulated rbLSC in both types of bioprinted scaffolds by flow cytometry with propidium iodide staining (supplementary figure S1(B)). Based on the results, the live cell ratios were 86.7 $\pm$ 1.6% in GelMA scaffolds and 92.1 $\pm$ 0.8% in HAGM scaffolds after seven days of culture. In brief, we were able to fabricate both GelMA- and HAGM-based scaffolds encapsulating viable primary rbLSCs using our DLP-based bioprinting system.

3.2. Encapsulated primary rbLSCs displayed active status in GelMA-based bioprinted scaffolds while exhibiting quiescence in HAGM-based bioprinted scaffolds

While both GelMA- and HAGM-based bioprinted scaffolds maintained viable encapsulated primary rbLSCs, the cells displayed different behaviors depending on which scaffold they were cultured in. More cell aggregates or colonies were observed in GelMA-based bioprinted scaffolds, while rbLSCs encapsulated with HAGM-based scaffolds largely remained as single-cells after six days of culture (supplementary figure S1(C)). These results suggest that the interaction between rbLSCs and their surrounding ECM in the different bioprinted scaffolds influenced the stem cell status following the encapsulation. To further explore the effect of the scaffold matrix material on LSC-ECM interaction, we first needed to control the stiffness. Our DLP-based bioprinting system enables us to control the mechanical properties of the fabricated hydrogel scaffolds via spatiotemporal regulation of light exposure [23, 24]. Mechanical testing of GelMA- and HAGM-based bioprinted scaffolds indicated positive linear correlation between the Young's modulus and the light exposure time in our printing system (figure 2(A), supplementary figure S1(D)). Based on the results, GelMA and HAGM scaffolds had a similar Young's modulus with the light exposure time set to 25 s which was adopted as the primary bioprinting parameters for subsequent experiments.

To investigate the behavior of LSCs in the different scaffolds, we examined the expression of various LSC markers. Immunofluorescence staining showed the expression of PAX6, an ocular lineage marker, in both

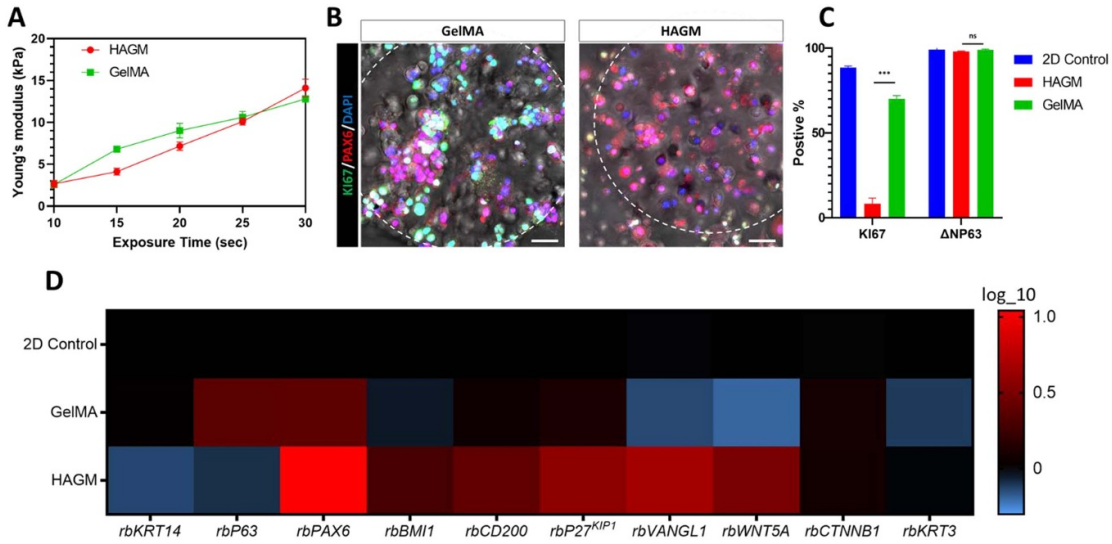

Figure 2. Encapsulated primary rbLSCs displayed different status in GelMA- or HAGM-based bioprinted scaffolds. (A) Linear plot of compressive modulus of the GelMA- or HAGM-based scaffolds versus the light exposure time (mean ± sd, n ⩾ 3); (B) representative images of immunofluorescence staining of proliferation marker KI67 and LSC lineage marker PAX6 on rbLSCs encapsulated in GelMA- or HAGM-based scaffolds after two days of culture (scale bars: 50 μm); (C) KI67-positive and ΔNP63-positve populations of the primary rbLSCs cultured in 2D and encapsulated in GelMA- or HAGM-based scaffolds after two days of culture as determined by flow cytometry (mean ± sd, n = 3); (D) heatmap of real-time qPCR data showing relative mRNA expression of LSC markers (KRT14, P63, PAX6, BMI1), LSC quiescent markers (CD200, $P27^{KIP1}$), corneal epithelium differentiation marker (KRT3), canonical WNT signaling pathway marker (CTNNB1) and non-canonical WNT signaling pathway markers (WNT5A, VANGL1) on rbLSCs on 2D surface or encapsulated in GelMA- or HAGM-based scaffolds after two days of culture.

GelMA- and HAGM-encapsulated rbLSCs while the expression of proliferation marker, KI67, was present only in the GelMA-based scaffolds (figure 2(B)). Consistently, flow cytometry identified significantly smaller percentage of KI67 positive rbLSCs encapsulated in HAGM-based bioprinted scaffolds compared to the population encapsulated in GelMA, while the positive ratio of stemness marker, ΔNP63, remained identical in both scaffolds (figure 2(C), supplementary figure S2(A)). The decreased KI67 positive population of rbLSCs encapsulated in HAGM-based bioprinted scaffolds can be reversed by releasing the cells from scaffolds (supplementary figure S2(B)). We have also performed transcriptional analysis with real-time qPCR to compare rbLSCs in 2D culture or encapsulation with GelMA- or HAGM-based bioprinted scaffolds (figure 2(D)). We found up-regulated mRNA expression of *PAX6* and *BMI1* in the HAGM group compared to the 2D control, while *P63* was up-regulated in the GelMA group. In addition, the expression of two previously reported LSC quiescence markers, *CD200* and $P27^{KIP1}$, were up-regulated in the HAGM group [41–43]. The expression of corneal epithelium differentiation marker, *KRT3*, was downregulated in the GelMA group and showed no significant change in the HAGM group in comparison with the 2D control. Furthermore, mRNA expression of markers of non-canonical WNT pathway, *VANGL1* and *WNT5A*, were up-regulated in the HAGM group but down-regulated in the GelMA group. Meanwhile, the expression of marker of canonical WNT pathway, *CTNNB1*, remained unchanged among the three groups. These results indicated the potential participation of non-canonical WNT pathway in the LSCs-ECM interactions [44–47]. Collectively, these results demonstrated an active status of the rbLSCs encapsulated in GelMA-based scaffolds and quiescent characteristics of rbLSCs in the HAGM-based scaffolds.

3.3. Encapsulated primary hLSCs were viable but displayed different status in GelMA- or HAGM-based scaffolds

Based on the ECM-dependent response of rbLSCs in the GelMA- or HAGM-based scaffolds, we further explored the LSC-ECM interaction in hLSCs. Primary hLSCs were isolated and expanded from human corneoscleral rims of three different donors and subjected to bioprinting with GelMA and HAGM, respectively. Similar to the rbLSCs, Live/Dead^{TM} staining showed that most of the encapsulated hLSCs remained viable in both types of bioprinted scaffolds during culture (figure 3(A)). Consistent with rbLSCs, aggregated colonies of hLSCs were largely found in the GelMA-based scaffolds but rarely observed in the HAGM-based scaffolds (figure 3(B)). Real-time qPCR showed that the hLSCs encapsulated in HAGM-based scaffolds had significantly higher expression of *PAX6, CD200* and $P27^{KIP1}$, while the expression of *KI67* was significantly down-regulated compared to the 2D control and the GelMA group (figure 3(C)). In addition, *KRT14* expression

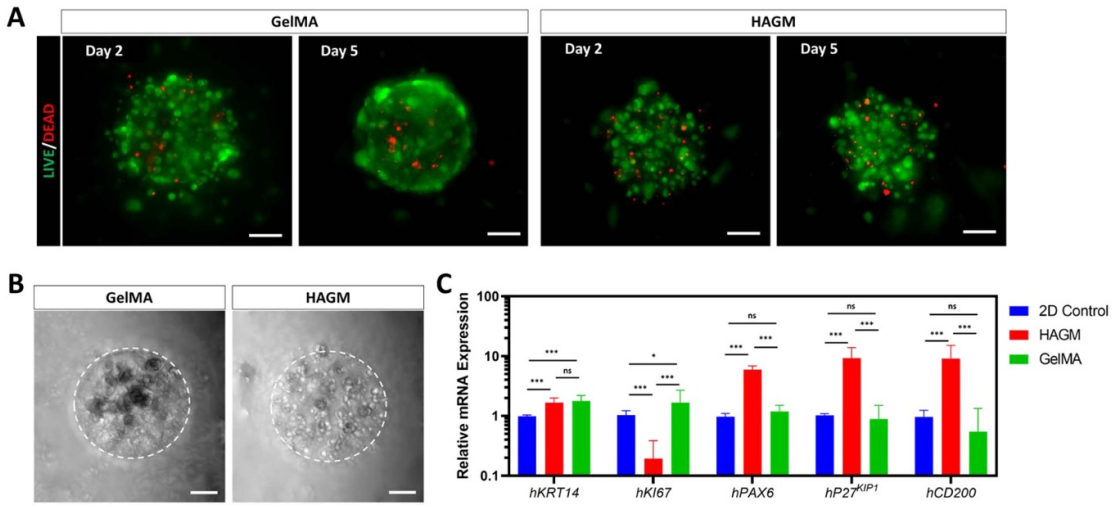

Figure 3. Encapsulated primary hLSCs remained viable and displayed different status in GelMA- or HAGM-based scaffolds. (A) Representative images of Live/Dead^{TM} staining of hLSCs encapsulated with GelMA- or HAGM-based scaffolds at day 2 and day 5 of culture (scale bars: 100 μm); (B) representative bright field images of bioprinted scaffolds with GelMA/HAGM encapsulating primary hLSCs after five days of culture (scale bars: 100 μm); (C) real-time qPCR data showing relative mRNA expression of proliferation marker (KI67), LSC markers (KRT14, PAX6), LSC quiescent markers (CD200, P27^{KIP1}) of the primary hLSCs on 2D surface or encapsulated in GelMA- or HAGM-based scaffolds after two days of culture (mean $\pm$ sd, n = 3).

was significantly up-regulated in both bioprinted groups comparing with the 2D control. These results reinforce the observation that LSCs respond differently (e.g. exhibiting active proliferation or quiescence) to the surrounding ECM composition, and appears to be consistent whether the LSCs are isolated from rabbits or humans, suggesting that this may be highly valuable for future clinical studies.

3.4. DLP-based bioprinting of dual ECM 'Yin-Yang' LSC model

After ascertaining the ECM-dependent active/quiescent status of encapsulated LSCs in GelMA- and HAGM-based scaffolds, we aimed to build a dual *in vitro* ECM model that could facilitate these differential statuses of cells within the same hydrogel, thus coming closer to recapitulating native LSC niches where cells in both activated/quiescent states coexist [3]. For this, we chose to utilize a 'Yin-Yang' pattern that allows for the placement of GelMA and HAGM distinctly separate yet spatially close regions. To demonstrate the feasibility of our design, we first printed the 'Yin-Yang' pattern in microscale with GelMA and HAGM mixed with fluorescence microspheres (figure 4(A)). Fluorescent microscopic imaging showed the precise patterning of the acellular hydrogel materials matching our design specification. In follow-up prints, we replaced fluorescent microspheres with primary rbLSCs and verified the status of the encapsulated rbLSCs in different parts of the dual ECM model (figure 4(B)). Immunofluorescence staining showed the positive expression of KI67 in the GelMA-based region while few KI67 positive cells were found in the HAGM-based region (figure 4(B)). Therefore, with our bioprinting method, we were able to fabricate the dual ECM 'Yin-Yang' model whose separate ECM-portions induced active/quiescent statuses for the LSC.

4. Discussion

With the recent technological advances in tissue engineering and regenerative medicine, stem cell therapies based on hydrogel scaffolds have become popular for the treatment of LSCD [12]. However, cost effective approaches for the high-throughput fabrication of hydrogel scaffolds encapsulating primary LSCs remains an active area of research. Furthermore, behavior that LSCs exhibit in response to different 3D matrices presents an attractive opportunity in formulating scaffolds that can effectively recapitulate the native microenvironment of the LSC niche. Our study demonstrated a novel engineering approach applying DLP-based bioprinting for the fabrication of hydrogel scaffolds encapsulating both rabbit and human primary LSCs. We successfully printed GelMA- and HAGM-based microscale hydrogel scaffolds that maintained the viability of the encapsulated primary rbLSCs. The cells exhibited ECM-dependent phenotypes with an active status in GelMA- and quiescent status in HAGM-based scaffolds. We repeated the bioprinting experiments with hLSCs and confirmed the consistency of the ECM-dependent phenotype in primary human cells. Moreover, we applied DLP-based bioprinting to build a dual ECM 'Yin-Yang' model encapsulating LSCs in active and quiescent status within the same culture.

3D engineered tissues are 3D fabricated biomimetic systems consisted of the corresponding cells from the target tissue and organ, as well as the

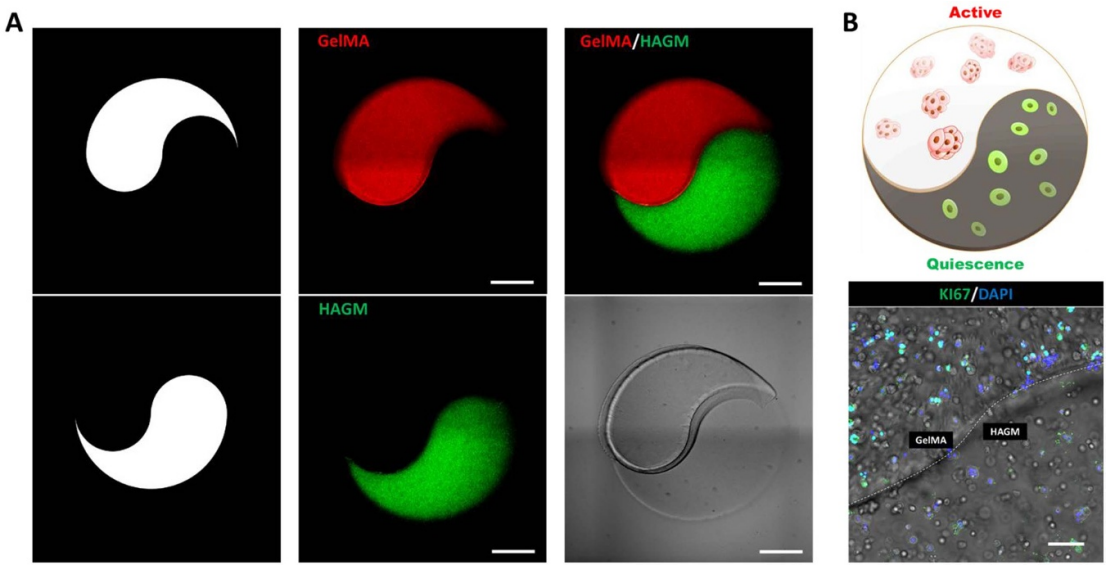

Figure 4. Bioprinting of a dual ECM 'Yin-Yang' model encapsulating rbLSCs. (A) Illustration of the design patterns and bright field images of the acellular dual ECM 'Yin-Yang' models encapsulating fluorescent microspheres (scale bars: 500 μm); (B) illustration and a representative image of immunofluorescence staining of KI67 on dual ECM 'Yin-Yang' model encapsulating primary rbLSCs after two days of culture (scale bars: 100 μm).

hydrogel scaffolds that mimic ECM [18, 48]. As the construct geometry and the cell distribution can be manipulated to recapitulate the physiological microenvironment, 3D engineered tissues could have better performance in applications like drug screening, disease modeling, and regenerative medicine compared to the 2D monolayer cell model [17, 19, 49]. Tissue regeneration using endogenous stem cell is a promising solution for many medical conditions [2, 28, 50, 51]. As the essential endogenous epithelial stem cell contributing to corneal regeneration, LSCs have been explored in various approaches in combination with hydrogel scaffolds for corneal epithelium reconstruction [52, 53]. DLP-based bioprinting has been instrumental in tissue engineering as it facilitated the fabrication of high-throughput hydrogel scaffolds encapsulating various types of stem cells [18]. We used DLP-based bioprinting to produce GelMA- or HAGM-based hydrogel scaffolds encapsulating primary rbLSCs and hLSCs. DLP-based bioprinting maintained the viability and stemness of the encapsulated LSCs in both materials. With flexible and precise control over morphological structures, the microscale hydrogel scaffolds encapsulating LSCs can be optimized by our bioprinting system to serve various therapeutic purposes including minimally invasive injectable stem cell transplantation [54]. In addition, the translucent nature of the GelMA and HAGM scaffolds not only enabled facile monitoring of cell morphology and behaviors, but also makes ideal candidates for corneal tissue-on-a-chip *in vitro* disease modeling. Although the bioprinted hydrogel scaffolds in this study were 2.5D constructs that have consistent pattern along the thickness direction, they were able to provide insightful information for disease modeling [17, 26]. In the future, we could use the DLP-based bioprinting system to fabricate true 3D constructs such as a corneal tissue with complex 3D features for various biomedical applications [55].

The ECM-dependent regulation and reprogramming of epithelial stem cell fate have been indicated as prevalent mechanisms in different tissues including epidermis, lung, intestine, colon and cornea [30, 56–59]. By controlling the matrix stiffness with our bioprinting system, we were able to compare the influence of ECM component on the encapsulated LSCs. As a result, we found that primary rbLSCs and hLSCs actively proliferated and formed aggregated colonies in the GelMA-based scaffolds while showed inhibited proliferation and aggregation in the HAGM-based scaffolds. Further analysis showed the active/quiescent status of encapsulated LSCs by comparing proliferation and stemness markers. The quiescence of LSCs in HAGM-based scaffolds can potentially be mediated by the HA-specific cell adhesion excluding integrins [60–62]. We also found the HAGM-encapsulated rbLSCs presented proliferative status after being released from scaffolds and cultured for a week, indicating that the HAGM-encapsulated rbLSCs were reversibly quiescent. Non-canonical WNT signaling pathways (planar cell polarity) have been reported to modify the activation/quiescence in multiple endogenous stem cells [46, 47, 63]. Notably, we found upregulated mRNA expression of markers related to non-canonical WNT signaling pathways in primary LSCs encapsulated in HAGM-based scaffolds, which is consistent with the previously reported

ECM-response of primary LSCs cultured on engineered HA scaffolds [38, 64]. As a proof-of-concept, we further combined these findings with multimaterial bioprinting to fabricate a dual ECM 'Yin-Yang' model simultaneously encapsulating primary LSCs in active/quiescent status. The dual ECM model can be an attractive platform for drug screening since it reproduced stem cell quiescence that was correlated to drug-resistance and recapitulated the stem cells in heterogeneous status that could react to drugs differently [65–67].

5. Conclusions

We applied DLP-based bioprinting to fabricate engineered microscale hydrogel scaffolds based on GelMA and HAGM. These scaffolds supported not only the viability of encapsulated primary rbLSCs and hLSCs, but also exhibited differential regulation. LSCs were found to display an ECM-dependent active/quiescent status as they actively proliferated in the GelMA-based scaffolds and took on quiescent characteristics in the HAGM-based scaffolds. A bioprinted dual-ECM 'Yin-Yang' model encapsulating both active and quiescent LSCs were fabricated based on these findings. Together, these results illustrated an innovative engineering approach for disease modeling, drug screening and the development of an LSC-based regenerative therapy for the treatment of LSCD and related ocular diseases. Future studies exploring other types of biomaterials or integrating different cell types would be valuable to investigate.

Data availability statement

The raw/processed data required to reproduce these findings can be shared by the authors upon request.

All data that support the findings of this study are included within the article (and any supplementary files).

Acknowledgments

We thank Kathleen Miller, Dr Claire Yu, Jiaao Guan, Wisarut Kiratitanaporn, Leilani Kwe, and Trevor Fried for their technical support. We also acknowledge the University of California San Diego School of Medicine Microscopy Core for the imaging equipment and the technical supports offered by the staff there. The UCSD School of Medicine Microscopy Core facility was supported by National Institutes of Health (NIH) Grant P30 NS047101. This work was supported in part by grants from the NIH to S C (R21EY031122, R01EB02185) and S D (R01EY021797), National Science Foundation (NSF) to S C (1937653), and California Institute for Regenerative Medicine to S D (CLIN1-08686 and CLIN2-11650). This material is based upon work supported by the NSF Graduate Research Fellowship Program under Grant Nos. DGE-1650112 (J S). Any opinions, findings, and conclusions or recommendations expressed in this material are those of the author(s) and do not necessarily reflect the views of the NSF.

Author contributions

Z Z, S D and S C conceived and initiated this project Z Z, A B and J T designed and performed the experiments, as well as analyzed experimental results Y X, H H, X W, X D, J B, Y S, C M, A S S Y, M T E Y and X S contributed to sample fabrication, processing, data gathering, and analysis. Z Z, A B and S C wrote the manuscript N S, S D and S C supervised the project.

Conflict of interest

The authors declare no competing financial interests.

ORCID iDs

Zheng Zhong https://orcid.org/0000-0003-4103-4752
Henry H Hwang https://orcid.org/0000-0001-6690-2929
Xiaoqian Deng https://orcid.org/0000-0002-4633-6314

References

[1] Dhouailly D, Pearton D J and Michon F 2014 The vertebrate corneal epithelium: from early specification to constant renewal *Dev. Dyn.* **243** 1226–41
[2] Ouyang H *et al* 2014 WNT7A and PAX6 define corneal epithelium homeostasis and pathogenesis *Nature* **511** 358–61
[3] Dziasko M A and Daniels J T 2016 Anatomical features and cell-cell interactions in the human limbal epithelial stem cell niche *Ocul. Surf.* **14** 322–30
[4] Bourne R R A *et al* 2017 Magnitude, temporal trends, and projections of the global prevalence of blindness and distance and near vision impairment: a systematic review and meta-analysis *Lancet Glob. Health* **5** 888–97
[5] Deng S X, Borderie V, Chan C C, Dana R, Figueiredo F C, Gomes J A P, Pellegrini G, Shimmura S and Kruse F E 2019 Global consensus on definition, classification, diagnosis, and staging of limbal stem cell deficiency *Cornea* **38** 364–75
[6] Le Q, Xu J and Deng S X 2018 The diagnosis of limbal stem cell deficiency *Ocul. Surf.* **16** 58–69
[7] Meller D *et al* 2000 Amniotic membrane transplantation for acute chemical or thermal burns *Ophthalmology* **107** 980–9
[8] Hopkinson A, McIntosh R S, Tighe P J, James D K and Dua H S 2006 Amniotic membrane for ocular surface reconstruction: donor variations and the effect of handling on TGF-β content *Investig. Ophthalmol. Vis. Sci.* **47** 4316–22
[9] Ramuta T Ž, Starčič Erjavec M and Kreft M E 2020 Amniotic membrane preparation crucially affects its broad-spectrum activity against uropathogenic bacteria *Front. Microbiol.* **11** 469
[10] Deng S X *et al* 2020 Global consensus on the management of limbal stem cell deficiency *Cornea* **39** 1291–302
[11] Mahdavi S S, Abdekhodaie M J, Mashayekhan S, Baradaran-Rafii A and Djalilian A R 2020 Bioengineering approaches for corneal regenerative medicine *Tissue Eng. Regen. Med.* **17** 567–93
[12] Nguyen K N, Bobba S, Richardson A, Park M, Watson S L, Wakefield D and Di Girolamo N 2018 Native and synthetic

scaffolds for limbal epithelial stem cell transplantation *Acta Biomater.* **65** 21–35
[13] Chen D, Qu Y, Hua X, Zhang L, Liu Z, Pflugfelder S C and Li D Q 2017 A hyaluronan hydrogel scaffold-based xeno-free culture system for ex vivo expansion of human corneal epithelial stem cells *Eye* **31** 962–71
[14] Sanie-Jahromi F, Eghtedari M, Mirzaei E, Jalalpour M H, Asvar Z, Nejabat M and Javidi-Azad F 2020 Propagation of limbal stem cells on polycaprolactone and polycaprolactone/gelatin fibrous scaffolds and transplantation in animal model *BioImpacts* **10** 44–54
[15] Soman P, Lee J W, Phadke A, Varghese S and Chen S 2012 Spatial tuning of negative and positive Poisson's ratio in a multi-layer scaffold *Acta Biomater.* **8** 2587–94
[16] Wang P, Li X, Zhu W, Zhong Z, Moran A, Wang W, Zhang K and Chen S 2018 3D bioprinting of hydrogels for retina cell culturing *Bioprinting* **12** e00029
[17] Tang M *et al* 2020 Three-dimensional bioprinted glioblastoma microenvironments model cellular dependencies and immune interactions *Cell Res.* **30** 833–53
[18] Yu C, Schimelman J, Wang P, Miller K L, Ma X, You S, Guan J, Sun B, Zhu W and Chen S 2020 Photopolymerizable biomaterials and light-based 3D printing strategies for biomedical applications *Chem. Rev.* **120** 10695–743
[19] Zhong Z *et al* 2021 Rapid bioprinting of conjunctival stem cell micro-constructs for subconjunctival ocular injection *Biomaterials* **267** 120462
[20] Qu X, Zhu W, Huang S, Li Y S, Chien S, Zhang K and Chen S 2013 Relative impact of uniaxial alignment vs. form-induced stress on differentiation of human adipose derived stem cells *Biomaterials* **34** 9812–8
[21] Soman P, Tobe B T D, Lee J W, Winquist A M, Singec I, Vecchio K S, Snyder E Y and Chen S 2012 Three-dimensional scaffolding to investigate neuronal derivatives of human embryonic stem cells *Biomed. Microdevices* **14** 829–38
[22] Wen J H, Vincent L G, Fuhrmann A, Choi Y S, Hribar K C, Taylor-Weiner H, Chen S and Engler A J 2014 Interplay of matrix stiffness and protein tethering in stem cell differentiation *Nat. Mater.* **13** 979–87
[23] Yu C, Ma X, Zhu W, Wang P, Miller K L, Stupin J, Koroleva-Maharajh A, Hairabedian A and Chen S 2019 Scanningless and continuous 3D bioprinting of human tissues with decellularized extracellular matrix *Biomaterials* **194** 1–13
[24] Ma X, Yu C, Wang P, Xu W, Wan X, Lai C S E, Liu J, Koroleva-Maharajh A and Chen S 2018 Rapid 3D bioprinting of decellularized extracellular matrix with regionally varied mechanical properties and biomimetic microarchitecture *Biomaterials* **185** 310–21
[25] Hribar K C, Choi Y S, Ondeck M, Engler A J and Chen S 2014 Digital plasmonic patterning for localized tuning of hydrogel stiffness *Adv. Funct. Mater.* **24** 4922–6
[26] Ma X *et al* 2016 Deterministically patterned biomimetic human iPSC-derived hepatic model via rapid 3D bioprinting *Proc. Natl Acad. Sci. USA* **113** 2206–11
[27] Gouveia R M and Connon C J 2020 Biomechanical modulation therapy—a stem cell therapy without stem cells for the treatment of severe ocular burns *Transl. Vis. Sci. Technol.* **9** 1–11
[28] Xia H, Li X, Gao W, Fu X, Fang R H, Zhang L and Zhang K 2018 Tissue repair and regeneration with endogenous stem cells *Nat. Rev. Mater.* **3** 174–93
[29] Ramos T, Scott D and Ahmad S 2015 An update on ocular surface epithelial stem cells: cornea and conjunctiva *Stem Cells Int.* **2015** 1–7
[30] Gouveia R M, Lepert G, Gupta S, Mohan R R, Paterson C and Connon C J 2019 Assessment of corneal substrate biomechanics and its effect on epithelial stem cell maintenance and differentiation *Nat. Commun.* **10** 1–17
[31] Chakraborty A, Dutta J, Das S and Datta H 2013 Comparison of ex vivo cultivated human limbal epithelial stem cell viability and proliferation on different substrates *Int. Ophthalmol.* **33** 665–70
[32] Bonnans C, Chou J and Werb Z 2014 Remodelling the extracellular matrix in development and disease *Nat. Rev. Mol. Cell Biol.* **15** 786–801
[33] Gesteira T F, Sun M, Coulson-Thomas Y M, Yamaguchi Y, Yeh L K, Hascall V and Coulson-Thomas V J 2017 Hyaluronan rich microenvironment in the limbal stem cell niche regulates limbal stem cell differentiation *Investigative Ophthalmol. Vis. Sci.* **58** 4407–21
[34] Cho I J, Lui P P W, Obajdin J, Riccio F, Stroukov W, Willis T L, Spagnoli F and Watt F M 2019 Mechanisms, hallmarks, and implications of stem cell quiescence *Stem Cell Rep.* **12** 1190–200
[35] Cooper J and Giancotti F G 2019 Integrin signaling in cancer: mechanotransduction, stemness, epithelial plasticity, and therapeutic resistance *Cancer Cell* **35** 347–67
[36] Wang Y A Z, Plane J M, Jiang P, Zhou C J and Deng W 2011 Concise review: quiescent and active states of endogenous adult neural stem cells: identification and characterization *Stem Cells* **29** 907–12
[37] Sagga N, Kuffová L, Vargesson N, Erskine L and Collinson J M 2018 Limbal epithelial stem cell activity and corneal epithelial cell cycle parameters in adult and aging mice *Stem Cell Res.* **33** 185–98
[38] Chen S-Y, Han B, Zhu Y-T, Mahabole M, Huang J, Beebe D C and Tseng S C G 2015 HC-HA/PTX3 purified from amniotic membrane promotes BMP signaling in limbal niche cells to maintain quiescence of limbal epithelial progenitor/stem cells *Stem Cells* **33** 3341–55
[39] Shirahama H, Lee B H, Tan L P and Cho N J 2016 Precise tuning of facile one-pot gelatin methacryloyl (GelMA) synthesis *Sci. Rep.* **6** 1–11
[40] Zhu W, Cui H, Boualam B, Masood F, Flynn E, Rao R D, Zhang Z Y and Zhang L G 2018 3D bioprinting mesenchymal stem cell-laden construct with core-shell nanospheres for cartilage tissue engineering *Nanotechnology* **29** 185101
[41] Vattulainen M, Ilmarinen T, Koivusalo L, Viiri K, Hongisto H and Skottman H 2019 Modulation of Wnt/BMP pathways during corneal differentiation of hPSC maintains ABCG2-positive LSC population that demonstrates increased regenerative potential *Stem Cell Res. Ther.* **10** 236
[42] Bojic S *et al* 2018 CD200 expression marks a population of quiescent limbal epithelial stem cells with holoclone forming ability *Stem Cells* **36** 1723–35
[43] Barbaro V, Testa A, Di Iorio E, Mavilio F, Pellegrini G and De Luca M 2007 C/EBPδ regulates cell cycle and self-renewal of human limbal stem cells *J. Cell Biol.* **177** 1037–49
[44] Mentink R A, Rella L, Radaszkiewicz T W, Gybel T, Betist M C, Bryja V and Korswagen H C 2018 The planar cell polarity protein VANG-1/Vangl negatively regulates Wnt/β-catenin signaling through a Dvl dependent mechanism *PLoS Genet.* **14** e1007840
[45] Katoh M 2017 Canonical and non-canonical WNT signaling in cancer stem cells and their niches: cellular heterogeneity, omics reprogramming, targeted therapy and tumor plasticity (Review) *Int. J. Oncol.* **51** 1357–69
[46] Chavali M, Klingener M, Kokkosis A G, Garkun Y, Felong S, Maffei A and Aguirre A 2018 Non-canonical Wnt signaling regulates neural stem cell quiescence during homeostasis and after demyelination *Nat. Commun.* **9** 1–17
[47] Sugimura R *et al* 2012 Noncanonical Wnt signaling maintains hematopoietic stem cells in the niche *Cell* **150** 351–65
[48] Et V, J D, W L, B L and L S 2018 Three-dimensional cell culture models for anticancer drug screening: worth the effort? *J. Cell. Physiol.* **233** 2993–3003
[49] Ma X, Liu J, Zhu W, Tang M, Lawrence N, Yu C, Gou M and Chen S 2018 3D bioprinting of functional tissue models for personalized drug screening and *in vitro* disease modeling *Adv. Drug Deliv. Rev.* **132** 235–51
[50] He L, Nguyen N B, Ardehali R and Zhou B 2020 Heart regeneration by endogenous stem cells and cardiomyocyte proliferation: controversy, fallacy, and progress *Circulation* **142** 275–91

[51] Lin H et al 2016 Lens regeneration using endogenous stem cells with gain of visual function *Nature* **531** 323–8
[52] Mobaraki M, Abbasi R, Vandchali S O, Ghaffari M, Moztarzadeh F and Mozafari M 2019 Corneal repair and regeneration: current concepts and future directions *Front. Bioeng. Biotechnol.* **7** 135
[53] Wright B, Mi S and Connon C J 2013 Towards the use of hydrogels in the treatment of limbal stem cell deficiency *Drug Discovery Today* **18** 79–86
[54] Selver Ö B, Yağcı A, Eğrilmez S, Gürdal M, Palamar M, Çavuşoğlu T, Ateş U, Veral A, Güven Ç and Wolosin J M 2017 Limbal stem cell deficiency and treatment with stem cell transplantation *Turk. J. Ophthalmol.* **47** 285
[55] Hwang H H et al 2020 High throughput direct 3D bioprinting in multiwell plates *Biofabrication* **13** 025007
[56] Daley W P, Peters S B and Larsen M 2008 Extracellular matrix dynamics in development and regenerative medicine *J. Cell Sci.* **121** 255–64
[57] Yui S et al 2018 YAP/TAZ-dependent reprogramming of colonic epithelium links ECM remodeling to tissue regeneration *Cell Stem Cell* **22** 35–49.e7
[58] Chermnykh E, Kalabusheva E and Vorotelyak E 2018 Extracellular matrix as a regulator of epidermal stem cell fate *Int. J. Mol. Sci.* **19** 1003
[59] Meran L, Baulies A and Li V S W 2017 Intestinal stem cell niche: the extracellular matrix and cellular components *Stem Cells Int.* **2017** 1–11
[60] Kim Y and Kumar S 2014 CD44-mediated adhesion to hyaluronic acid contributes to mechanosensing and invasive motility *Mol. Cancer Res.* **12** 1416–29
[61] Lam J, Truong N F and Segura T 2014 Design of cell-matrix interactions in hyaluronic acid hydrogel scaffolds *Acta Biomater.* **10** 1571–80
[62] Frith J E, Mills R J and Cooper-White J J 2012 Lateral spacing of adhesion peptides influences human mesenchymal stem cell behaviour *J. Cell Sci.* **125** 317–27
[63] Zheng M, Tian C, Fan T and Xu B 2019 Fibronectin regulates the self-renewal of rabbit limbal epithelial stem cells by stimulating the Wnt11/Fzd7/ROCK non-canonical Wnt pathway *Exp. Eye Res.* **185** 107681
[64] Tseng S C G, Chen S Y, Mead O G and Tighe S 2020 Niche regulation of limbal epithelial stem cells: HC-HA/PTX3 as surrogate matrix niche *Exp. Eye Res.* **199** 108181
[65] Chen W, Dong J, Haiech J, Kilhoffer M C and Zeniou M 2016 Cancer stem cell quiescence and plasticity as major challenges in cancer therapy *Stem Cells Int.* **2016** 1–16
[66] De Angelis M L, Francescangeli F, La Torre F and Zeuner A 2019 Stem cell plasticity and dormancy in the development of cancer therapy resistance *Front. Oncol.* **9** 626
[67] Rehman S K et al 2021 Colorectal cancer cells enter a diapause-like DTP state to survive chemotherapy *Cell* **184** 226–242.e21